Scripta Materialia 273 (2026) 117111

Contents lists available at ScienceDirect

Scripta Materialia

journal homepage: www.journals.elsevier.com/scripta-materialia

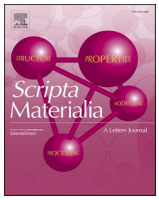

Distinct impacts of hydrogen and carbon on thermally activated dislocation motion in Fe-Cr-Ni austenitic steel

Haruki Nishida [a,b,*], Yuhei Ogawa [b], Akinobu Shibata [b,c]

[a] Graduate School of Science and Technology, University of Tsukuba, 1-1-1 Tennnodai, Tsukuba, Ibaraki 305-8577 Japan
[b] Research Center for Structural Materials, National Institute for Materials Science (NIMS), 1-2-1 Sengen, Tsukuba, Ibaraki 305-0047, Japan
[c] Institute of Pure and Applied Sciences, University of Tsukuba, 1-1-1 Tennnodai, Tsukuba, Ibaraki 305-8577 Japan

ARTICLE INFO

Keywords:
Thermally activated processes
Strain rate sensitivity
Hydrogen
Carbon
Austenitic steels

ABSTRACT

Plastic flow behavior and strain rate sensitivity, S, of Fe-15Cr-15Ni (mass%) austenitic steel, alloyed with either hydrogen or carbon, were evaluated by tensile and stress relaxation tests at ambient temperature. The effects of these two interstitial elements on solid solution-hardening and thermally activated dislocation motion were compared in terms of *Haasen plot*—S versus flow stress. Both hydrogen and carbon exhibited solid solution-hardening of the same order of magnitude, increasing S proportionally with their concentrations. However, their ability to increase S was distinct. Hydrogen caused a much steeper increase in S, acting as extremely localized obstacles resisting dislocation motion. In contrast, despite exhibiting comparable solid solution-hardening, carbon led to an order of magnitude smaller increase in S than hydrogen. This result demonstrates a relatively long-range and less rate-sensitive nature of carbon, which is totally different from hydrogen in its obstacle character.

Introduction

Solid solution-hardening by interstitial carbon and nitrogen in face-centered cubic (FCC) metals/alloys is $G/1200$~$G/800$ (G: shear modulus) per atomic concentration of solutes [1–5]—an order of magnitude greater than the strengthening by substitutional elements [5,6]. This difference in strengthening ability is generally attributed to larger lattice distortion around a solution site of an interstitial atom [5]. In contrast, although its lattice distortion [7] is only one-fourth of those around carbon and nitrogen [8], we recently revealed that hydrogen, also an interstitial element, induces solid solution-hardening comparable to that by carbon and nitrogen in Fe-Cr-Ni austenitic steels [9–11]. Although the effect is favorable for austenitic steels currently used for hydrogen energy-related infrastructures, such abnormal strengthening due to hydrogen cannot be explained by lattice distortion theory alone. To comprehend the solid solution-hardening by a series of interstitial elements, a refined understanding of the mechanisms governing solute-dislocation interactions is desired.

Plastic deformation proceeds as dislocations overcome short-range obstacles (solute atoms and forest dislocations in the case of solution-hardened FCC alloys) with the synergistic aid of applied stress and thermal vibration—thermally activated dislocation motion [12]. One can define activation volume in such a process, $V = bdL$, as the area swept by a dislocation segment during each activation event, dL, multiplied by Burgers vector, b, where d is obstacle width, L is obstacle interspacing. Strain rate sensitivity, $S = \partial\tau^*/\partial\ln\dot{\gamma}$, where τ^* is effective shear stress and $\dot{\gamma}$ is shear strain rate, is inversely proportional to V. These two parameters, measurable by transient mechanical tests (e.g., stress relaxation or creep), are useful to investigate dislocation-obstacle interaction mechanisms [13–17]. To extract the contribution of solute atoms in a field combined with forest dislocations, another powerful tool is the so-called *Haasen plot*—S values measured along stress-strain curves are plotted against flow stress [14,15,18]. Such analysis was applied to alloys hardened by substitutional only [19–22] or by both substitutional and interstitial [14,23]. However, no application of Haasen plot focusing on the intrinsic role of interstitials has been attempted. Ogawa et al. have filled in this blank by employing Haasen plot to study thermally activated deformation behavior in AISI Type310S (Fe-24Cr-19Ni) steel containing hydrogen [24,25]. Their findings demonstrated the essential function of hydrogen to significantly increase S, successively diminishing the contribution of forest dislocations to deformation kinetics. These results suggest that hydrogen plays a role as an extremely localized obstacle sensitive to thermal activation,

* Corresponding author.
E-mail address: NISHIDA.Haruki@nims.go.jp (H. Nishida).

https://doi.org/10.1016/j.scriptamat.2025.117111
Received 24 October 2025; Received in revised form 17 November 2025; Accepted 18 November 2025
Available online 22 November 2025

while its similarity/dissimilarity with other interstitials remain unknown.

To deepen our understanding of solid solution-hardening by interstitial elements in light of thermally activated dislocation motion, this study comparatively investigates the influences of carbon—common element in austenitic steels—and hydrogen in Fe-Cr-Ni alloy system. Stress relaxation tests were conducted to measure V and S in an identical base composition of Fe-15Cr-15Ni, alloyed with various concentrations of hydrogen or carbon. Subsequent use of Haasen plot uncovered, for the first time, distinct forms of these two interstitials as obstacles resisting dislocations.

In a thermally activated process, the energy supplied by thermal vibration, ΔG, which assists dislocation motion, is a function of zero-stress activation energy, ΔG_0, effective shear stress acting on the dislocation, τ^*, and V [12,17]:

$$\Delta G = \Delta G_0 - \tau * V \tag{1}$$

The shear strain rate, $\dot{\gamma}$, under the ΔG follows an Arrhenius-type rate equation using a pre-exponential factor $\dot{\gamma}_0$ that involves vibrational frequency of dislocation segment, mobile dislocation density, and average interspacing between dispersed obstacles on the slip plane [12,17]:

$$\dot{\gamma} = \dot{\gamma}_0 \exp\left(-\frac{\Delta G}{kT}\right) \tag{2}$$

where k is Boltzmann constant and T is absolute temperature. By taking stress-derivative of ΔG in Eqs. (1) and (2), and combining together, an inversely proportional relationship between S and V is obtained [13,17]:

$$S = \frac{\partial \tau *}{\partial \ln \dot{\gamma}} = \frac{kT}{V} \tag{3}$$

when solute concentration is significantly higher than forest dislocation density, flow stress is approximated by linear superposition of the matrix frictional stress due to solutes, τ_s, and the strain-hardening component due to forest dislocations, τ_d, $\tau = \tau_s + \tau_d$ [15,26]. Accordingly, S is also expressed as a sum of their derivatives–S_s and S_d:

$$S = S_s + S_d = \frac{\partial \tau_s}{\partial \ln \dot{\gamma}} + \frac{\partial \tau_d}{\partial \ln \dot{\gamma}} = \frac{\partial \tau_s}{\partial \ln \dot{\gamma}} + \frac{\partial \ln \tau_d}{\partial \ln \dot{\gamma}} \tau_d = \frac{\partial \tau_s}{\partial \ln \dot{\gamma}} + \frac{\partial \ln \tau_d}{\partial \ln \dot{\gamma}} \left(\tau - \tau_y\right) \tag{4}$$

here, τ_y is shear yield stress. In Haasen plot, S values are plotted against $\tau - \tau_y$. In terms of Eq. (4), the intercept on the vertical axis and the slope of Haasen plot reflect the solutes and the forest dislocation components of S, respectively. Note that here, S represents the strain rate sensitivity of flow stress in units of MPa, and should not be confused with the dimensionless strain rate sensitivity, $\partial \ln \tau / \partial \ln \dot{\gamma}$, typically denoted by m [22,27].

The base chemical composition of the investigated alloy was Fe-15Cr-15Ni (mass %). In addition to the base alloy, two carbon-added alloys with 0.46 and 0.92 at % (hereafter referred to as 0.46C and 0.92C, respectively) were prepared. 10 kg ingots cast by vacuum induction melting were hot-forged and caliber-rolled into 10 mm-square rods. The rods were finally solution-treated at 1473 K for 1 h and quenched in water, yielding a fully austenitic microstructure with average grain size of 500 μm (Appendix A1). This large grain size reduces the fraction of interstitial solute atoms that segregate to grain boundaries and minimizes their influence on the solute concentrations within grains. Cylindrical tensile specimens with a gauge diameter of 4 mm and a gauge length of 30 mm were machined, the surface of their gauge section was mirror-finished by polishing with 1 μm diamond suspension. Some specimens of the base alloy were exposed to hydrogen gas at pressures of 10 or 100 MPa and a temperature of 543 K for 130 h. This treatment resulted in uniform hydrogen distribution through the specimen's gauge sections with concentrations of 0.13 (0.13H) and 0.42 (0.42H) at % as measured by thermal desorption spectroscopy (Appendix A2).

Tensile tests with and without intermittent stress relaxations were conducted at 295±1 K by a screw-driven electromechanical test frame with 20 kN load capacity. Elongations were measured by a contact-type strain gauge extensometer with a gauge length of 25 mm. The strain rate was 10^{-4}/s, and the machine crosshead was held for 300 s at nominal strain, ε_n, interval of 0.02. Using initial 30 s of each relaxation data, V was determined by fitting to the following logarithmic relaxation law [16,28]:

$$\Delta \tau = -\frac{kT}{V} \ln\left(\frac{t}{c} + 1\right) \tag{5}$$

where $\Delta \tau$ is the relaxed stress (negative quantity), t is the relaxation time, and c is a constant. The measured normal stress was translated into shear stress by a Taylor factor of polycrystalline FCC metals: 3.06.

True stress-true strain curves obtained from monotonic tensile tests are shown in Fig. 1(a), and the enhancement of yield stress (0.2 % proof stress) by hydrogen or carbon are plotted against solute concentrations in Fig. 1(b). Fig. 1(b) also includes the previously reported data for several hydrogen-charged commercial Fe-Cr-Ni steels (open symbols) [10,11], as well as carbon-added Fe-15Cr-15Ni steels (dashed and dashed-dotted lines) [1,2]. The hydrogen-induced solid solution-hardening was proportional to atomic hydrogen concentration, with a magnitude of approximately 80 MPa/at %, consistent with our prior works [10,11]. Similarly, carbon-induced solid solution-hardening also escalated proportionally to solute concentration with a slope of approximately 60 MPa/at %, also reproducing the previous reports [1,2]. Although their strengthening abilities were the same order of magnitude, strengthening by hydrogen was 20 MPa/at. % greater than that by carbon. For both hydrogen and carbon, their strengthening effects were significantly greater than the general solid solution-hardening by substitutional elements [5,6].

In Fig. 2(a)-(d), some examples of stress relaxation curves at true strain, ε_t, of 0.10, 0.18, 0.26, and 0.34 (nominal strain, ε_n, of 0.1, 0.2, 0.3, and 0.4) are shown wherein stress and time at the start of each relaxation were taken as the origin. Increasing hydrogen and carbon concentrations both amplified the magnitude of stress relaxation at a given strain. Notably, 0.42H exhibited greater relaxation than 0.92C although the solute concentration of 0.42H was lower than 0.92C.

V was determined by Eq. (5) (Appendix A4), followed by calculating S *via* Eq. (3). Fig. 3(a) shows the resultant Haasen plot. The base alloy yielded a straight line with positive intercept and slope. According to Eq. (4), this positive intercept reflects the contributions of alloying elements—Cr and Ni. Then, after involvement of carbon and hydrogen, the Haasen plot exhibited overall upward shift—increase in intercept—as the solute concentrations were increased. However, while such an intercept-increase by carbon remained minor, that by hydrogen was quite substantial. To quantify the impacts of each solute species, the intercepts of Haasen plot in Fig. 3(a) are reproduced as a function of solute concentration in Fig. 3(b), in which the data of hydrogen-charged Fe-24Cr-19Ni (Type310S) steel [24] are included. As for the solid solution-hardening in Fig. 1(b), the intercept-increase by carbon and hydrogen followed proportional concentration-dependences. However, the corresponding increasing rate—the slope of the lines in Fig. 3(b)—was 0.26 MPa/at % for carbon, whereas it exceeded 2 MPa/at % for hydrogen in both Fe-15Cr-15Ni and Fe-24Cr-19Ni alloys. This indicates that hydrogen enhanced S to an extent order of magnitude greater than carbon. Meanwhile, although carbon hardly affected the Haasen plot slope, hydrogen caused its slight decrease, the possible reason of which has been discussed in the authors' previous publication [24].

Although hydrogen and carbon exhibited solid solution-hardening of the same order of magnitude, their impacts on deformation kinetics differed markedly. Specifically, the increase in S per at % hydrogen was an order of magnitude greater than that for carbon (Fig. 3(b)). This

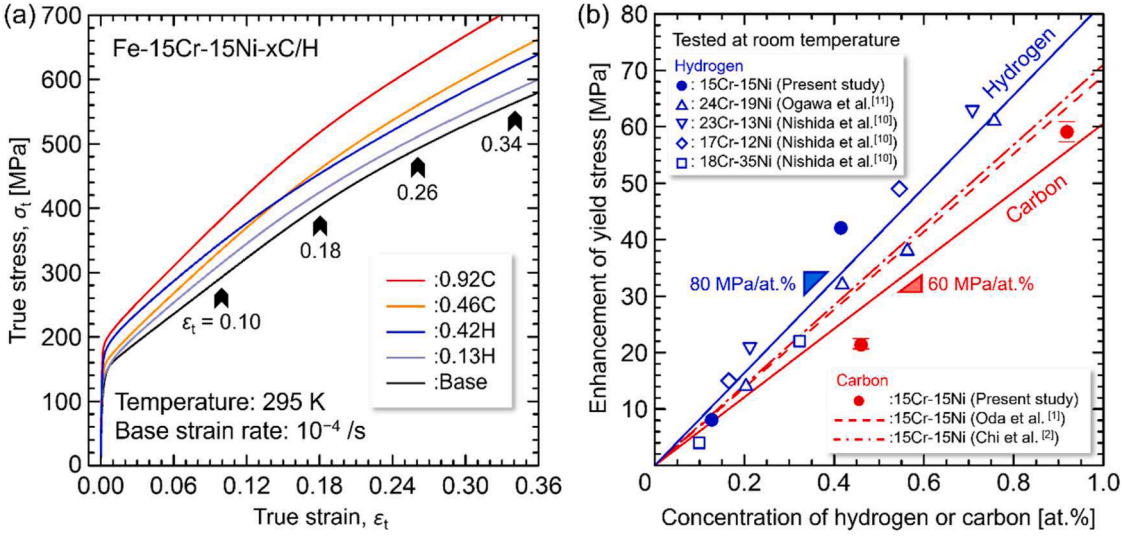

Fig. 1. (a) True stress-true strain curves obtained from monotonic tensile tests for the base, 0.46C, 0.92C, 0.13H, and 0.42H alloys. (b) enhancement of yield stress—magnitude of solid solution-hardening—by hydrogen and carbon as a function of solute concentration. the previously reported data of various hydrogen-charged and carbon-alloyed Fe-Cr-Ni austenitic steels [1,2,10,11] are also included in (b).

significant difference in S between hydrogen- and carbon-added alloys implies that hydrogen acts as thermal obstacle sensitive to strain rate variation, whereas carbon acts as more spatially extended, relatively rate-insensitive obstacle. Note that, in the study field of hydrogen-material interactions, there has also been a belief that hydrogen conversely enhances thermally activated movement of dislocations in FCC metals and alloys [29,30]. However, our series of recent papers critically revisited such a foregoing interpretation, no less emphasizing the net effect of hydrogen to retard dislocation motion at least in Fe-Cr-Ni austenitic steels [24,25,31].

Given the inverse relationship between S and V (eq. (3)), V for the dislocation surmounting hydrogen is smaller than that for carbon, indicating that hydrogen must have either a smaller d or L, or both. Indeed, the V calculated from the slope in Fig. 3(b)—increase in S per at % solute—*via* eq. (3) is $120b^3$ for hydrogen and $1000b^3$ for carbon. Contrarily, V estimated from the average interspacing of solutes randomly dispersed on the slip plane with a concentration $C_0 = 1$ at % (e.g., $(3^{1/2}b^2/4C_0)^{1/2}$ [32]) is approximately $10b^3$, significantly smaller than the experimental values. Such a discrepancy between experiments and estimations was also noted by Basinski et al. for substitutional solutes in Cu alloys [32]. They assumed a synergistic participation of multiple solute atoms in a single thermal activation event, urging us to consider a similar plural obstacle mechanism particularly for carbon.

Regarding thermally activated dislocation motion with hydrogen, Ogawa et al. proposed *diffusion-controlled glide* mechanism [24] combined with the *trough model* of solid solution-hardening proposed by Kocks [33]. Fig. 4(a) schematically illustrates this model. Owing to their high diffusivity even at ambient temperature, hydrogen atoms segregate into dislocation core, reducing the dislocation's line energy and tension. When shear stress is applied, dislocations tend to advance *via* forming a small bulge by dragging those segregated hydrogen. Although the bulge size is locally restricted by segregated hydrogen, the participation of multiple hydrogen atoms in a single bulge *via* statistical and collective diffusion jumps makes it reasonable that the experimental V is larger than the estimation based on the average interspacing. An essential requirement for such *diffusion-controlled glide* is that solute atoms are sufficiently mobile to coordinatively follow the dislocation movement. In the stress relaxation tests in this study with a strain rate of 10^{-4}/s, the dislocation velocity estimated from Orowan's equation is 10^{-10}~10^{-8} m/s (Appendix A5) [34,35]. At 295 K, the migration velocity of hydrogen, calculated from the diffusion coefficient [36], is on the order of 10^{-8} m/s, enabling its dynamic interaction with mobile dislocations. Meanwhile, for carbon, the migration should be so slow—order of 10^{-17} m/s [37]. Thus, a different form of interaction with dislocations must be considered.

Carbon-related V was an order of magnitude greater than that for hydrogen (Fig. 3(b)); besides, it was two orders greater than the prediction from an assumption of random solute dispersion. A plausible explanation for such a large V is the presence of carbon clusters or interstitial-substitutional (*i-s*) complexes, which aligns with the premise that multiple solute atoms may synergistically be involved in a single activation event. Several studies have reported the formation of *i-s* complexes in carbon-containing Fe-Cr-Ni austenitic steels. Shibata et al. conducted low-cycle fatigue tests on Fe-20Cr-15Ni and Fe-15Cr-15Ni alloys with ~0.3 mass % carbon and demonstrated that greater carbon contents promoted fatigue softening and planar dislocation glide [38]. They inferred the fragmentation of C—Cr complexes penetrated by dislocations, which renders the subsequent dislocations movement on the same slip plane easier. Oda et al. analyzed the effect of carbon on lattice distortion in Fe-15Cr-15Ni using X-ray diffraction and found a peak broadening potentially stemming from lattice distortion due to C—Cr complexes [1]. The alloys used in these studies were solution-treated at 1300 °C for 1 h, comparable to solution-treatment used here (i.e., at 1200 °C for 1 h). Thus, similar presence of C—Cr complexes is also likely in the present alloys. At elevated temperatures during solution treatment (or cooling period in quenching process), carbon can segregate around stochastically Cr-enriched zone. As the size of C—Cr complexes—obstacle to dislocations—evolves, both d and L should become larger. Therefore, the V significantly larger than the prediction from random dispersion seems feasible and reasonable.

The stability of *i-s* complexes depends on an electrochemical interaction energy arising from interstitial-substitutional affinity—0.1 eV for C—Cr [39]. Meanwhile, first-principles calculations by Moriyama et al. showed that replacing one Fe atom with Cr around octahedral site in austenite reduces hydrogen absorption energy by 0.05 eV [40], suggesting that hydrogen can also form H—Cr complexes. This is likely because hydrogen in dislocation cores, driven by its stronger binding energy with dislocations (0.14 eV [41]), plays a more dominant role in thermally activated dislocation motion than H—Cr complexes in lattice.

Fig. 4(b) schematically illustrates thermally activated dislocation motion in carbon-containing alloys based on the context above. In the presence of spatially extended C—Cr complexes, dislocations sweep a

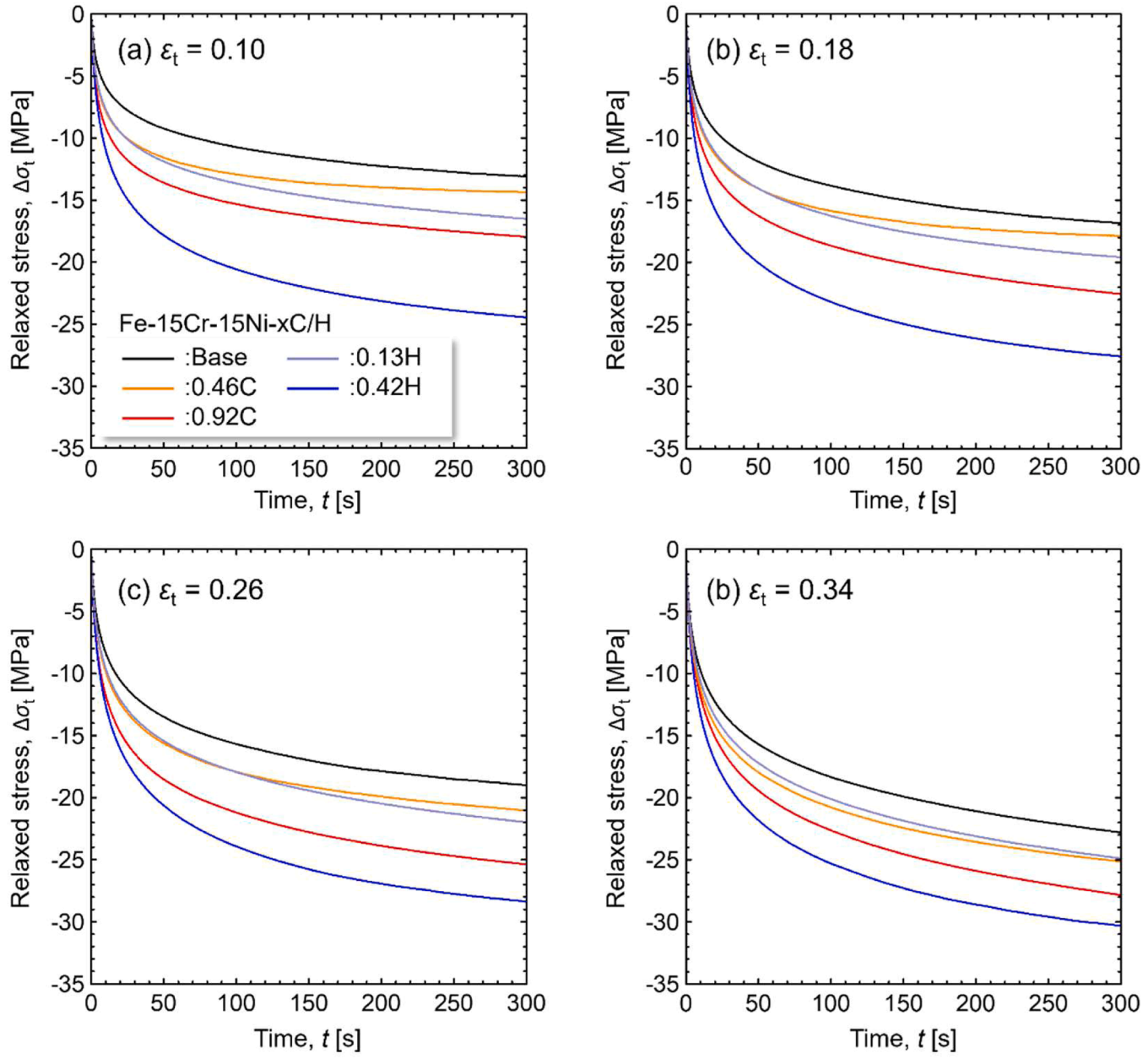

Fig. 2. Stress relaxation curves of the base, 0.46C, 0.92C, 0.13H, and 0.42H alloys at ε_t = (a) 0.10, (b) 0.18, (c) 0.26, and (d) 0.34 (corresponding to ε_n = 0.1, 0.2, 0.3, and 0.4). these strain levels are marked by the black arrows in Fig. 1(a).

larger area in a single activation event than in the presence of dense hydrogen along dislocation core (Fig. 4(a)). Such a difference in obstacle size and distribution influences not only *V* but also *S*. The corresponding obstacle potential profiles for hydrogen and carbon are virtually shown in Fig. 4(c) and (d) to visualize the stress variations with strain rate changes. A decrease in strain rate leads to a stochastic increase in ΔG, giving dislocations more chance to overcome obstacles *via* thermal vibration. As ΔG increases, the effective stress to overcome the obstacle correspondingly decreases. When considering the increase in ΔG by a fixed amount, more localized obstacles lead to a larger reduction in effective stress. The variation in *S* for hydrogen and carbon in Fig. 3(b) reflects this intrinsic difference in obstacle character.

In summary, the effects of carbon and hydrogen in Fe-15Cr-15Ni austenitic steels on solid solution-hardening and thermally activated deformation were investigated by evaluating *S via* Haasen plot. Both carbon and hydrogen caused solid solution-hardening of the same order of magnitude, proportional to their concentrations. Although both elements increased Haasen plot intercept (i.e., solute contribution to *S*), the increase per at % solute was an order of magnitude higher for hydrogen than for carbon. This indicates that hydrogen plays a role as a localized thermal obstacle to dislocation motion. Contrarily, carbon acts as a more extended and widely dispersed obstacle, relatively insensitive to thermal activation. Despite the same order of magnitude solid solution-hardening, their strengthening mechanisms are mutually distinct in terms of thermally activated dislocation motion.

CRediT authorship contribution statement

Haruki Nishida: Writing – original draft, Investigation. **Yuhei Ogawa:** Writing – review & editing, Supervision. **Akinobu Shibata:** Writing – review & editing, Supervision.

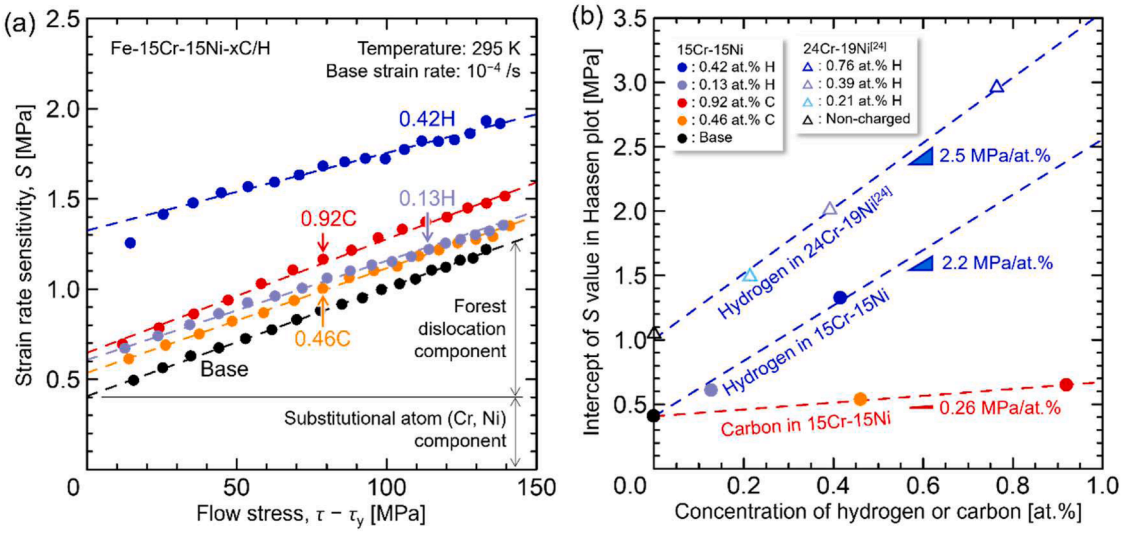

Fig. 3. (a) Haasen plot–strain rate sensitivity, *S*, versus flow stress. the intercept of the vertical axis in (a) is plotted against solute concentration in (b). the data of hydrogen-charged Fe-24Cr-19Ni investigated in the previous study [24] are included in (b).

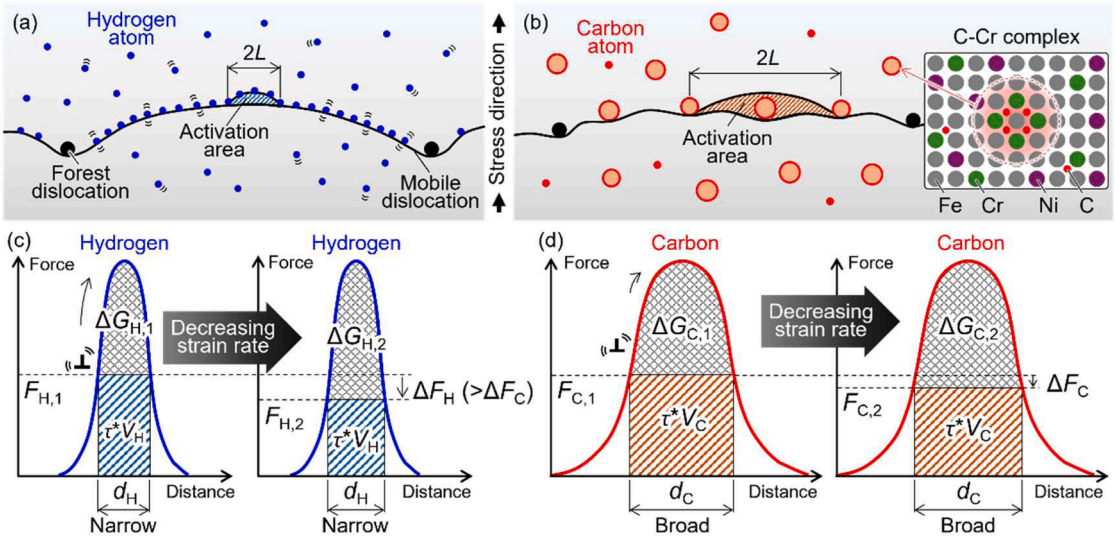

Fig. 4. Schematic illustrations of thermally activated dislocation motion in materials containing solute (a) hydrogen and (b) carbon. (c) and (d) virtually describe the obstacle profiles of these two types of interstitial elements. The variation in effective obstacle width causes the difference in strain rate sensitivity, *S*.

Declaration of competing interest

The authors declare that they have no known competing financial interests or personal relationships that could have appeared to influence the work reported in this paper.

Acknowledgement

This work was financially supported by JSPS KAKENHI (Grant No 24K17180) and Iketani Science and Technology Foundation (Grant No 0371199-A).

Supplementary materials

Supplementary material associated with this article can be found, in the online version, at doi:10.1016/j.scriptamat.2025.117111.

References

[1] K. Oda, N. Kondo, K. Shibata, X-ray absorption fine structure analysis of interstitial (C, N)-substitutional (Cr) complexes in austenitic stainless steels, ISIJ Int. 30 (1990) 625–631, https://doi.org/10.2355/isijinternational.30.625.
[2] B.-H. Chi, T. Nakazawa, K. Shibata, Effects of alloying elements on hardening and restoration behavior of 15Cr-15Ni high hardness non-magnetic stainless steel, ISIJ Int. 30 (1990) 615–624, https://doi.org/10.2355/isijinternational.30.615.
[3] M.L.G Byrnes, M. Grujicic, W.S. Owen, Nitrogen strengthening of a stable austenitic stainless steel, Acta Metall. 35 (1987) 1853–1862, https://doi.org/10.1016/0001-6160(87)90131-3.
[4] E. Werner, Solid solution and grain size hardening of nitrogen-alloyed austenitic steels, Mater. Sci. Eng. A 101 (1988) 93–98, https://doi.org/10.1016/0921-5093(88)90054-8.
[5] N. Ohkubo, K. Miyakusu, Y. Uematsu, H. Kimura, Effect of alloying elements on the mechanical properties of the stable austenitic stainless steel, ISIJ Int 34 (1994) 764–772, https://doi.org/10.2355/isijinternational.34.764.
[6] R.L. Fleischer, Substitutional solution hardening, Acta Metall. 11 (1963) 203–209, https://doi.org/10.1016/0001-6160(63)90213-X.
[7] T. Ito, Y. Ogawa, W. Gong, W. Mao, T. Kawasaki, K. Okada, A. Shibata, S. Harjo, Role of solute hydrogen on mechanical property enhancement in Fe–24Cr–19Ni austenitic steel: an in situ neutron diffraction study, Acta Mater. 287 (2025) 120767, https://doi.org/10.1016/j.actamat.2025.120767.

[8] H.M. Ledbetter, M.W. Austin, Dilation of an fcc Fe–Cr–Ni alloy by interstitial carbon and nitrogen, Mater. Sci. Technol. 3 (1987) 101–104, https://doi.org/10.1179/mst.1987.3.2.101.
[9] Y. Ogawa, H. Hosoi, K. Tsuzaki, T. Redarce, O. Takakuwa, H. Matsunaga, Hydrogen, as an alloying element, enables a greater strength-ductility balance in an Fe-Cr-Ni-based, stable austenitic stainless steel, Acta Mater. 199 (2020) 181–192, https://doi.org/10.1016/j.actamat.2020.08.024.
[10] H. Nishida, Y. Ogawa, K. Tsuzaki, Chemical composition dependence of the strength and ductility enhancement by solute hydrogen in Fe–Cr–Ni-based austenitic alloys, Mater. Sci. Eng. A 836 (2022) 142681, https://doi.org/10.1016/j.msea.2022.142681.
[11] Y. Ogawa, O. Takakuwa, K. Tsuzaki, Solid-solution hardening by hydrogen in Fe–Cr–Ni-based austenitic steel: temperature and strain rate effects, Mater. Sci. Eng. A 879 (2023) 145281, https://doi.org/10.1016/j.msea.2023.145281.
[12] D. Hull, D.J. Bacon, Introduction to Dislocations, 3rd ed., Elsevier, 2011 https://doi.org/10.1016/C2009-0-64358-0.
[13] F. Guiu, P.L. Pratt, Stress relaxation and the plastic deformation of solids, Phys. Status Solidi 6 (1964) 111–120, https://doi.org/10.1002/pssb.19640060108.
[14] R.A. Mulford, Analysis of strengthening mechanisms in alloys by means of thermal-activation theory, Acta Metall. 27 (1979) 1115–1124, https://doi.org/10.1016/0001-6160(79)90129-9.
[15] U.F. Kocks, Superposition of alloy hardening, strain hardening, and dynamic recovery. Strength of Metals and Alloys, Elsevier, 1979, pp. 1661–1680, https://doi.org/10.1016/B978-1-4832-8412-5.50250-2.
[16] P. Groh, R. Conte, Stress relaxation and creep in α-iron filamentary single crystals at low temperature, Acta Metall. 19 (1971) 895–902, https://doi.org/10.1016/0001-6160(71)90082-4.
[17] A.G. Evans, R.D. Rawlings, The thermally activated deformation of crystalline materials, Phys. Status Solidi 34 (1969) 9–31, https://doi.org/10.1002/pssb.19690340102.
[18] P. Haasen, Plastic deformation of nickel single crystals at low temperatures, Philos. Mag. 3 (1958) 384–418, https://doi.org/10.1080/14786435808236826.
[19] S. Saimoto, The characterization of materials by precision strain rate sensitivity, J. Eng. Mater. Technol. 109 (1987) 230–235, https://doi.org/10.1115/1.3225969.
[20] S. Saimoto, B.J. Diak, Advanced method for structure-strength-ductility assessment of dispersion-strengthened FCC metals using activation work, mean slip distance and constitutive relation analyses: decoding the Haasen plot, Mater. Sci. Eng. A 828 (2021) 142119, https://doi.org/10.1016/j.msea.2021.142119.
[21] B.J. Diak, S. Saimoto, The determination of solute clusters in dilute aluminum alloys using strain rate sensitivity, Mater. Sci. Eng. A 234–236 (1997) 1019–1022, https://doi.org/10.1016/S0921-5093(97)00342-0.
[22] W.A. Curtin, New interpretation of the Haasen plot for solute-strengthened alloys, Scr. Mater. 63 (2010) 917–920, https://doi.org/10.1016/j.scriptamat.2010.07.003.
[23] R.A. Mulford, U.F. Kocks, New observations on the mechanisms of dynamic strain aging and of jerky flow, Acta Metall. 27 (1979) 1125–1134, https://doi.org/10.1016/0001-6160(79)90130-5.
[24] Y. Ogawa, M. Tanaka, T. Fujita, A. Shibata, Thermally activated dislocation motion in hydrogen-alloyed Fe–Cr–Ni austenitic steel revisited via Haasen plot, Int. J. Hydrog. Energy 74 (2024) 170–182, https://doi.org/10.1016/j.ijhydene.2024.06.113.
[25] Y. Ogawa, T. Fujita, Solid solution-hardening by hydrogen in Fe–Cr–Ni-based austenitic steel studied by strain rate sensitivity measurement: contributions of effective stress and solute drag, Mater. Sci. Eng. A 911 (2024) 146941, https://doi.org/10.1016/j.msea.2024.146941.
[26] Y. Dong, T. Nogaret, W.A. Curtin, Scaling of dislocation strengthening by multiple obstacle types, Met. Mater. Trans. Phys. Met. Mater. Sci. 41 (2010) 1954–1960, https://doi.org/10.1007/s11661-010-0229-z.
[27] S. Mishra, V.K. Beura, A. Singh, M. Yadava, Effect of obstacle strength and spacing on the slope of Haasen plot, Mater. Sci. Technol. 35 (2019) 403–408, https://doi.org/10.1080/02670836.2019.1567043.
[28] P. Feltham, Stress relaxation in magnesium at low temperatures, Phys. Status Solidi 3 (1963) 1340–1346, https://doi.org/10.1002/pssb.19630030805.
[29] E. Sirois, H.K. Birnbaum, Effects of hydrogen and carbon on thermally activated deformation in nickel, Acta Metall. Mater. 40 (1992) 1377–1385, https://doi.org/10.1016/0956-7151(92)90438-K.
[30] D.P. Abraham, C.J. Altstetter, Hydrogen-enhanced localization of plasticity in an austenitic stainless steel, Metall. Mater. Trans. A 26 (1995) 2859–2871, https://doi.org/10.1007/BF02669644.
[31] Y. Ogawa, A. Shibata, Plastic flow in Fe-Cr-Ni austenitic steel under the presence of solute H: a study via room temperature creep, Acta Mater. 285 (2025) 120659, https://doi.org/10.1016/j.actamat.2024.120659.
[32] Z.S. Basinski, R.A. Foxall, R. Pascual, Stress equivalence of solution hardening, Scr. Metall. 6 (1972) 807–814, https://doi.org/10.1016/0036-9748(72)90052-X.
[33] U.F. Kocks, Kinetics of solution hardening, Metall. Trans. A 16 (1985) 2109–2129, https://doi.org/10.1007/BF02670415.
[34] T.H. Alden, Theory of mobile dislocation density: application to the deformation of 304 stainless steel, Metall. Trans. A 18 (1987) 51–62, https://doi.org/10.1007/BF02646221.
[35] Y. Estrin, L.P. Kubin, Local strain hardening and nonuniformity of plastic deformation, Acta Metall. 34 (1986) 2455–2464, https://doi.org/10.1016/0001-6160(86)90148-3.
[36] Y. Mine, T. Kimoto, Hydrogen uptake in austenitic stainless steels by exposure to gaseous hydrogen and its effect on tensile deformation, Corros. Sci. 53 (2011) 2619–2629, https://doi.org/10.1016/j.corsci.2011.04.022.
[37] F. Ernst, A. Avishai, H. Kahn, X. Gu, G.M. Michal, A.H. Heuer, Enhanced carbon diffusion in austenitic stainless steel carburized at low temperature, Met. Mater. Trans. Phys. Met. Mater. Sci. (2009) 1768–1780, https://doi.org/10.1007/s11661-009-9854-9.
[38] K. Shibata, M. Kogita, C.S. Chen, T. Fujita, Effects of carbon and silicon on softening in low-cycle fatigue of austenitic stainless steels, Trans. Iron Steel Inst. Jpn. 28 (1988) 406–412, https://doi.org/10.2355/isijinternational1966.28.406.
[39] V.G. Gavriljuk, H. Berns, High Nitrogen Steels, Springer Berlin Heidelberg, Heidelberg, Berlin, 1999, https://doi.org/10.1007/978-3-662-03760-7.
[40] J. Moriyama, O. Takakuwa, M. Yamaguchi, Y. Ogawa, K. Tsuzaki, The contribution of Cr and Ni to hydrogen absorption energy in Fe-Cr-Ni austenitic systems: a first-principles study, Comput. Mater. Sci. 232 (2024) 112650, https://doi.org/10.1016/j.commatsci.2023.112650.
[41] A. Atrens, N.F. Fiore, K. Miura, Dislocation damping and hydrogen pinning in austenitic stainless steels, J. Appl. Phys. 48 (1977) 4247–4251, https://doi.org/10.1063/1.323410.